The EMBO Journal (2006) 25, 3156–3166 | © 2006 European Molecular Biology Organization | All Rights Reserved 0261-4189/06
www.embojournal.org

THE EMBO JOURNAL

Structure of stem-loop IV of *Tetrahymena* telomerase RNA

Yu Chen[1], Jessica Fender[1], Jason D Legassie[2], Michael B Jarstfer[2], Tracy M Bryan[3] and Gabriele Varani[1,4,*]

[1]Department of Chemistry, University of Washington, Seattle WA, USA, [2]Division of Medicinal Chemistry and Natural Products, University of North Carolina, Chapel Hill, NC, USA, [3]Children's Medical Research Institute, Westmead, NSW, Australia and [4]Department of Biochemistry, University of Washington, Seattle WA, USA

Conserved domains within the RNA component of telomerase provide the template for reverse transcription, recruit protein components to the holoenzyme and are required for enzymatic activity. Among the functionally essential domains in ciliate telomerase RNA is stem-loop IV, which strongly stimulates telomerase activity and processivity even when provided in *trans*. The NMR structure of *Tetrahymena thermophila* stem-loop IV shows a highly structured distal stem-loop linked to a conformationally flexible template-proximal region by a bulge that severely kinks the entire RNA. Through extensive structure–function studies, we identify residues that contribute to both these structural features and to enzymatic activity, with no apparent effect on the binding of TERT protein. We propose that the bending induced by the GA bulge and the flexibility of the template-proximal region allow positioning of the prestructured apical loop during the catalytic cycle.

The EMBO Journal (2006) **25,** 3156–3166. doi:10.1038/sj.emboj.7601195; Published online 15 June 2006
Subject Categories: RNA; structural biology
Keywords: NMR; RNA structure; ribonucleoprotein; stem-loop; telomerase

Introduction

Telomeres are DNA–protein complexes that cap the end of linear chromosomes and enhance their genetic stability by protecting the DNA ends from recombination, degradation and fusion with other chromosomes (Blasco *et al*, 1997; Lee *et al*, 1998; Lingner and Cech, 1998; de Lange and Jacks, 1999). The natural loss of telomeres that occurs during normal cell division is counteracted by the *de novo* addition of telomeric repeats carried out by telomerase. This enzyme has two core components: a protein (TERT) and an RNA (TER) (Blasco *et al*, 1999). TERT is the catalytic subunit and shares homology to viral reverse transcriptases (Lingner *et al*, 1997), whereas TER contains the template (Feng *et al*, 1995). The holoenzyme contains other accessory proteins (Mitchell *et al*, 1999; Seto *et al*, 1999; Witkin and Collins, 2004; O'Connor *et al*, 2005; Prathapam *et al*, 2005), but they are less well conserved than TERT and dispensable for basal enzymatic activity. However, many of these proteins are required for activity *in vivo* as they control ribonucleoprotein assembly and maturation or its subnuclear localization (Mitchell *et al*, 1999; Wang and Meier, 2004).

TERT protein is highly conserved, whereas TER varies in size, secondary structure and sequence among different organisms (Chen *et al*, 2000; Zappulla *et al*, 2005). TER provides the template sequence for reverse transcription as well as a landing pad to organize ribonucleoprotein assembly during RNP maturation and in the fully catalytic mature enzyme (Zappulla and Cech, 2004). Despite variations in sequence and length, some secondary structure elements appear to share common functional roles in ciliates, yeast and vertebrates, suggesting that the basic biochemical activities of telomerase RNA are well conserved (Chen *et al*, 2000; Zappulla *et al*, 2005).

All TERs contain three major domains with shared functions that are most clearly defined in vertebrates (Chen *et al*, 2000). The 5′-end of vertebrate and ciliate TERs contains the template and a pseudoknot that plays key roles in enzymatic activity (Figure 1). The 3′-end of vertebrate telomerase RNAs contains a highly conserved elongated hairpin (CR4–CR5 domain). It is essential for telomerase catalytic activity and defines a second site of interaction with TERT protein (Tesmer *et al*, 1999; Mitchell and Collins, 2000; Chen *et al*, 2002). The vertebrate CR4–CR5 domain has a possible functional counterpart in the ciliate stem-loop IV (Mason *et al*, 2003), the subject of the present investigation. *Tetrahymena thermophila* provides a well-established model system for understanding how telomerase functions. Its RNA subunit contains four conserved double helices (I–IV) (Figure 1A) (Bhattacharyya and Blackburn, 1994; Lingner *et al*, 1994). Stem I bridges the 5′- and 3′-ends of the molecule, whereas stems II and IIIa/IIIb are necessary for TERT binding to telomerase RNA, for telomerase activity *in vitro* and for ribonucleoprotein (RNP) assembly *in vivo*. Stem-loop IV functions in the correct folding of the stem III pseudoknot and makes a major contribution to telomerase enzyme activity (Sperger and Cech, 2001) and to repeat addition processivity (Lai *et al*, 2003). Deletion of the complete stem-loop, mutations of conserved residues in the apical loop and deletion of the GA bulge, all dramatically reduce telomerase activity (Autexier and Greider, 1998; Sperger and Cech, 2001). Remarkably, activity can be restored by the addition of stem-loop IV *in trans* (Mason *et al*, 2003). The apical loop of stem IV may interact directly with the N-terminus of TERT protein (O'Connor *et al*, 2005), whereas the region more proximal to the template in secondary structure (Figure 1A), together with the GA bulge, interact with protein p65 (Witkin and Collins, 2004; O'Connor *et al*, 2005; Prathapam *et al*, 2005;

*Corresponding author. Departments of Chemistry & Biochemistry, University of Washington, Box 351700, Seattle, WA 98185-1700, USA. Tel: +1 206 543 7113; Fax: +1 206 685 8665;
E-mail: varani@chem.washington.edu

Received: 12 January 2006; accepted: 15 May 2006; published online: 15 June 2006

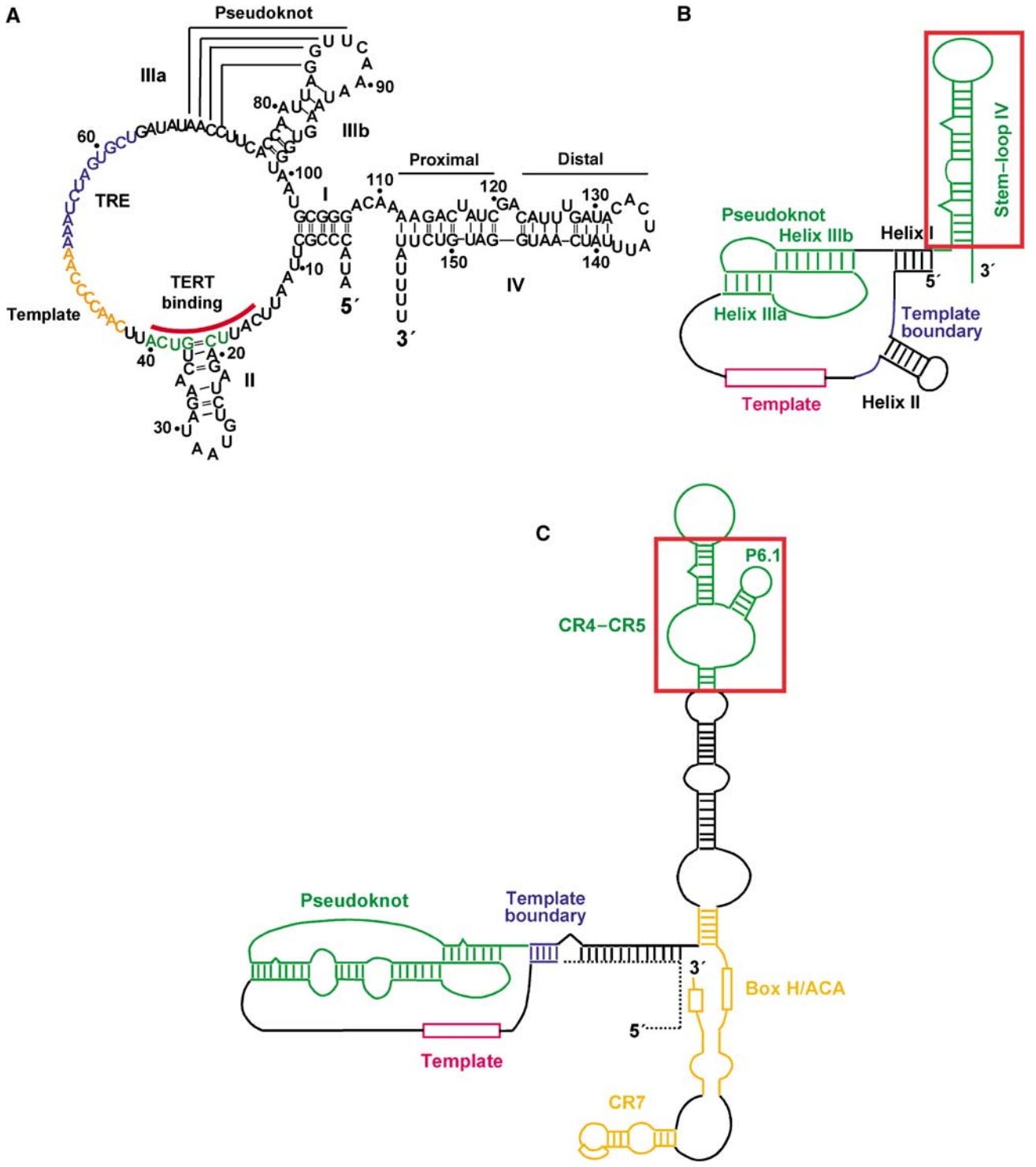

Figure 1 Secondary structures of telomerase RNAs. (**A**) Sequence and secondary structure of *T. thermophila* telomerase RNA. Regions of known function are colored and labeled; TRE, template recognition element. Comparison of secondary-structure models of (**B**) ciliate and (**C**) vertebrate telomerase RNAs; functionally equivalent regions are colored similarly; stem-loop IV and the CR4–CR5 domain are boxed in red squares.

O'Connor and Collins, 2006). The association of p65 with TER enhances the binding affinity of TERT to TER (Prathapam *et al*, 2005; O'Connor and Collins, 2006).

The essential roles of *T. thermophila* stem-loop IV in telomerase enzymatic activity prompted us to study its structure. The NMR structure presented here shows a highly structured distal stem-loop linked to a flexible template-proximal region by a conserved GA bulge that severely kinks the entire RNA. Mutations designed to investigate the structure–function relationship of stem-loop IV identify nucleotides within the apical loop that severely compromise catalytic activity but do not affect recruitment of TERT

protein. Based on these results, we propose that the kink induced by the GA bulge, and the flexibility of the lower part of the structure, affect catalytic activity by positioning the apical loop during catalysis.

Results

Structure determination

Initial studies of the full-length 43-nucleotide stem-loop IV (tet43-full) (Figure 2A) revealed substantial spectral overlap even when samples were prepared with selective isotopic labeling of either AU or GC nucleotides. The sequence of stem-loop IV is very AU rich and conformational exchange for the lower part of the structure further complicated data analysis (see below). In order to maximize the quality of the final structure, we adopted the divide-and-conquer method that represents a well-established approach to determine RNA structures by NMR (Greatorex *et al*, 2002; Lukavsky *et al*, 2003). The complete 43-nucleotide stem-loop IV was divided into two parts corresponding to the template-proximal (tet43-bot) and distal (tet43-top) parts of the stem-loop (Supplementary Figure 1). A three base-pair overlap was retained to merge the two substructures during structure calculation. In order to establish whether the excised secondary structure elements maintain the same conformation as in the complete stem-loop IV, we compared NMR chemical shifts of common residues in the three RNA constructs. Nucleotides covering the apical part of the structure have virtually identical chemical shifts as those observed for the same positions in the full-length RNA, whereas residues within the template-proximal oligonucleotide are also generally very similar to those observed in the full-length RNA (Supplementary Figure 1D). The small changes are consistent with minor differences due to the conformational exchange observed in this region of the structure (see below). Thus, the same structures are formed in each of the fragments, validating the use of the divide-and-conquer method.

The solution structure of the full stem-loop IV of *Tetrahymena* telomerase RNA was determined by merging distance and dihedral angle restraints obtained from each of the two substructures (and for the complete RNA) with residual dipolar coupling (RDC) restraints obtained for the full-length RNA, as described in the Materials and methods section. As shown in Table I, over 30 constraints per residue were collected. Of 100 calculated structures, 30 had no NOE violation greater than 0.5 Å or dihedral violations greater than 5°; we chose the 20 structures with the lowest constraint violation to represent the ensemble of conformations of stem-loop IV. Importantly, the inclusion of RDCs in the structure calculation improved significantly the overall precision of the structure; the r.m.s.d. for the ensemble was reduced from 3.65 to 1.96 Å. Structural statistics for the final ensemble of 20 best structures are presented in Table I and a superposition of the 10 lowest energy structures is shown in Figure 2B.

Structure of Tetrahymena telomerase RNA stem-loop IV

The RNA forms a severely kinked structure, with the apical part of the stem-loop rigidly defined and capped by a highly structured 7-nucleotide (CACUAUU) loop (Figure 2B and C). As a single-axis system and common alignment tensor could be used to refine the complete RNA structure using RDCs (see

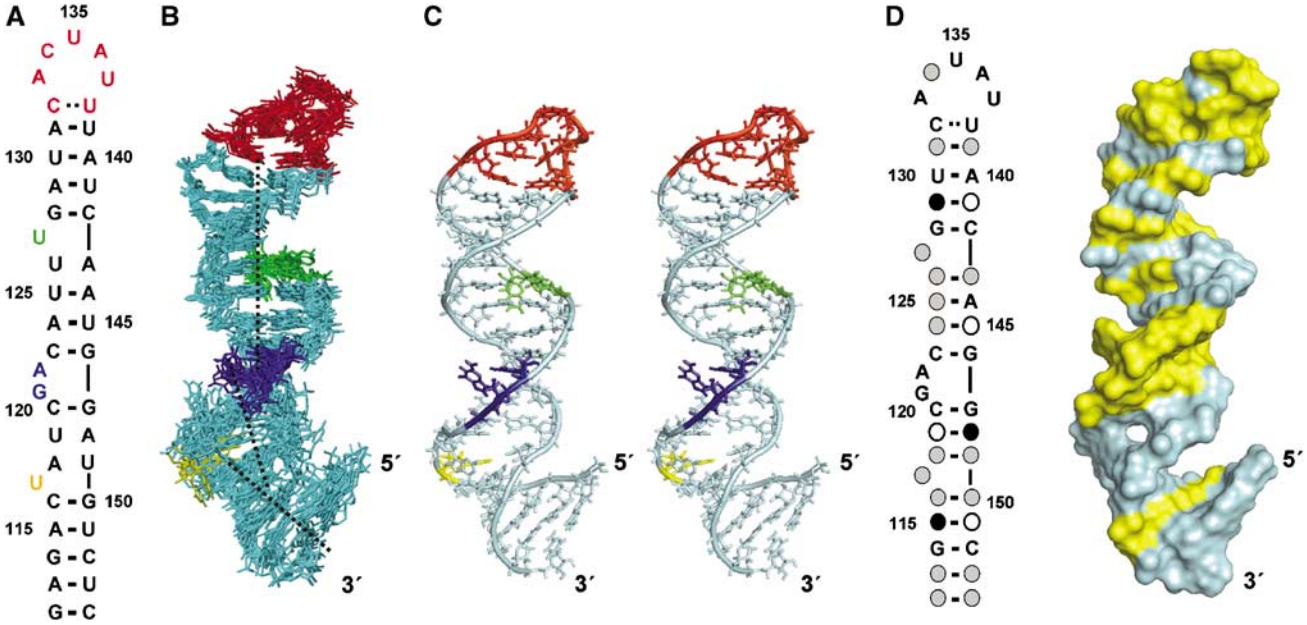

Figure 2 Structure of the *T. thermophila* telomerase RNA stem-loop IV. (**A**) Sequence and secondary structure of the stem-loop IV used in the current study. Bars connecting residues represent Watson–Crick hydrogen bonded pairs conclusively established by NMR. (**B**) Superposition (all heavy atoms) of the 10 structures of lowest energy, viewed down the minor groove of the heptaloop. Loop residues are colored in red, whereas bulged residues are colored as follows: U117 (yellow), G121–A122 (blue) and U126–U127 (green). Dotted black lines indicate the local helix axis to highlight the kink induced by the GA bulge and a second, smaller distortion, below the bulged U117. Structural figures are prepared by either MOLMOL (Koradi *et al*, 1996) or PyMOL (De Lano, 2002). (**C**) Stereo-view of the lowest energy structure with the backbone identified by a ribbon. (**D**) Phylogenetic conservation of residues in stem-loop IV among 17 *Tetrahymenine* ciliates (Ye and Romero, 2002). Variable nucleotides in the secondary structure are depicted as either pyrimidines (open circles) and purines (closed circles) or any nucleotide (gray circles). Absolutely conserved residues are colored yellow on surface of the structure.

Table I Constraints and structural statistics

Total number of restraints	1334
NOE-derived distance restraints[a]	952
Dihedral angles	250
Hydrogen bonding distance restraints	64
Base-pair planarity restraints	24
Dipolar couplings	44
Average r.m.s.d. from experimental restraints—20 structures	
Distance	0.0285
Dihedral	0.583
RDC	2.30
Average r.m.s.d. from ideal geometries—20 structures	
Bonds	0.00356
Angles	0.819
Impropers	0.337
Heavy atom r.m.s.d. from average structure (Å)—20 structures	
All RNA	1.95 (from mean)
Loop region	0.67 (132–138)
Apical stem-loop	0.76 (128–142)
Double-helical regions	0.54 (128–131, 139–142)
	0.87 (123–126, 143–146)
	2.3 (117–122. 147–149)
	0.74 (113–116, 150–153)

[a]Only structurally useful intraresidue distance restraints, involving protons separated by more than three bonds, are included.
RDC, residual dipolar coupling.

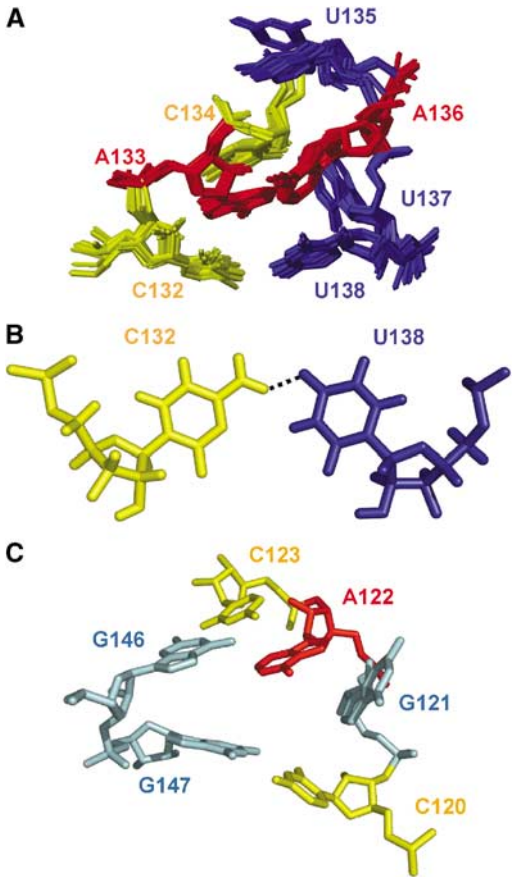

Figure 3 Structures of functionally important elements of stem-loop IV. (**A**) The ensemble of 10 lowest energy conformers for the heptaloop, viewed down the minor groove. Adenines are red; guanines are cyan; cytosines are yellow and uridines are blue. (**B**) The C·U base pair, with a dotted line indicating the putative hydrogen bond stabilizing the base pair. (**C**) Structure of the G121–A122 bulge.

Materials and methods), the kink in stem-loop IV is a rigid distortion and not a dynamic property.

The apical loop is the most conserved region of stem-loop IV, and its conformation is very well defined by a large number of internucleotide NOEs (r.m.s.d. 0.67 Å over 20 structures, Figure 3A). The bases of C132, A133, C134 and U138 continue double helical-like stacking into the loop and a C132–U138 base pair is consistently observed during the structure calculations, with a single hydrogen bond linking C132-NH and U138-O4 (Figure 3B). We note that the structure calculations were conducted without adding any hydrogen-bonding constraint for these two nucleotides. The base-pairing scheme is similar to a C·U base pair reported before in A-RNA duplex (Cruse *et al*, 1994), although the distance between C-N3 and U-N3H is too short (3.2 Å compared to 4.1 Å) to accommodate an additional water-mediated hydrogen-bonding interaction; it is likely that this difference simply reflects a limitation of the NMR method (water molecules cannot be directly observed). The Watson–Crick faces of the A133, C134, U135, A136 and U137 bases are all exposed to solvent (Figure 3A). In contrast, the hydrophobic faces of U137 and U138, as well as the C2 of A133 and A136, point towards each other and form a small hydrophobic patch at the center of the loop. The base of U135 at the very tip of the loop is less precisely defined by the data, yet it is completely exposed in all structures. U137 is on the opposite side of the phosphate backbone to A136, almost perpendicular to A133 and C134 and with the Watson–Crick edge facing the solvent. U138 stacks on U139 and forms a base-pairing interaction with C132. Several residues in the apical loop (U135, A136, U137 and U138) exhibited slightly increased $T_{1\rho}$ compared to the double-helical regions (Supplementary Figure 2), indicative of increased ps-ns motion. However, only U135 at the very tip of the loop had a significantly increased $T_{1\rho}$ value, consistent with this nucleotide having very few NOE contacts and a conformation that is not well defined in the final structural calculations. Those bases (C132, A133 and C134) that retain stacking in the loop generally have lower $T_{1\rho}$ values compared to the rest of the loop bases.

The bulged U127 base interrupts an otherwise perfect eight base-pair helix and bends the RNA but only slightly (by about 10°). We observe two populations of bulged conformers with either U126 or U127 flipping out in different calculated structures, both consistent with the experimental constraints. When U126 is the bulged residue, a single hydrogen-bonding interaction is observed between U127-NH and A143-N1 (2.1 Å) and neither U126 nor U127 forms base stacking interactions. When U127 is bulged out, U126 stacks on U125 instead and no hydrogen-bonding interactions are observed between U126 and A143. The sugars of nucleotides A124 to U127 are all in exchange between N- and S-type conformations, supporting the observation of conformational exchange. The A143 base continues stacking with C142 and A144 in all structures. Owing to the position of A143, U126 can only partially stack on U125 when U127 is flipped out.

RNAse V1 (that cleaves stacked or base paired residues) only cleaves weakly near the U127 bulge (Bhattacharyya and Blackburn, 1994), consistent with the formation of a weak base pair and conformation exchange at U127. However, deletion of the C123–U127 region only affected telomerase activity slightly and this bulge is not well conserved (Mason *et al*, 2003).

The GA bulge in the middle of stem-loop IV sharply kinks the entire structure (about 43°, as calculated using CURVES; Lavery and Sklenar, 1988). The A122 base remains stacked with C123, whereas G121 is completely bulged out generating the kink (Figure 3C). We emphasize that this distortion represents a rigid reorientation of the structure and not dynamic averaging, as we were able to refine the entire structure with RDCs using a single set of orientational parameters (see Materials and methods). The local bulge structure is also consistent with existing chemical and enzymatic mapping data. The bulged G121 makes the groove accessible to RNAse T1 (Bhattacharyya and Blackburn, 1994), an enzyme that cleaves single-stranded guanines. A122 is sensitive to diethylpyrocarbonate (DEPC), a chemical that modifies exposed adenines. The U117 bulged base is extrahelical and further kinks the helix axis.

To our surprise, formation of the two predicted A·U base pairs between the bulged U117 and G121–A122 (A118–U149; U119–A148) could not be confirmed by either water NOESY or HNN-COSY data. As a consequence, no hydrogen bonding constraint was introduced in the structural calculation for these nucleotides: the structures presented in the paper are calculated without base-pair constraints for A118–U149 and U119–A148. However, NOESY cross-peaks within each strand are consistent with the bases remaining stacked as in A-form helices. Consistent with the structural instability of this region, correlated experiments indicate that the sugars of U119, C120, G147 and A148 are all in exchange between N- and S-type conformations (data not shown). Conformational exchange is also apparent in the behavior of nonexchangeable resonances. For example, the H5–H6 cross-peak of U149 is extremely broad at 25°C, but becomes much sharper at 35°C. Furthermore, analysis of the base imino resonances indicates that the structural instability of these base pairs also affects nearby base pairs. The imino peak of G150 is broad at low temperature (2°C), but becomes much sharper at temperatures above 10°C.

Although conformational exchange is observed in the region between bulges U117 and G121–A122, $T_{1\rho}$ values were not increased compared to other parts of the structure (Supplementary Figure 2), suggesting that motion occurs on a time scale slower than ns but faster than μs-ms. However, when RDCs are plotted against the stem-loop IV secondary structure (Supplementary Figure 3), couplings measured for the bases in the region proximal to the GA bulge (A118–U149, U119–A148) have smaller values than the rest of the structure, indicating that conformational averaging due to local flexibility is occurring (Al-Hashimi *et al*, 2002). A similar attenuation in RDCs is also observed for the bases in the loop region, except for the C·U pair. RDC values attenuated by conformational averaging were not used in structural refinement. Nonetheless, RDCs for nucleotides close to the 5′- and 3′-ends are not attenuated, indicating that the relative orientation of the apical and lowest part of the structure is rigidly defined.

The sequence of the *Tetrahymena* telomerase stem-loop IV starts with 5′-AAGAC (and complementary bases at the 3′-end) (Figure 1A), whereas our oligonucleotide model starts with a G·C (instead of A·U) base pair to improve RNA transcription yield. When we prepared a sample starting with GAAGAC (identical to the *T. thermophila* sequence, except that a G instead of A is present 5′ to the first A·U base pair), 2D water NOESY spectra showed that the template-proximal stem region adopts the same A-form structure for both sequences (data not shown).

We reasoned that conformational exchange could perhaps be relieved by the addition of divalent metal ions, which often stabilize RNA structures (Allain and Varani, 1995; Cate *et al*, 1997). However, we only observed general broadening of imino resonances at increased Mg^{2+} concentration (up to 10 mM) due to nonspecific interaction of Mg^{2+} with the phosphate backbone and Mg^{2+}-induced RNA aggregation, as is often observed. No new imino peaks appeared and no significant chemical shift changes occurred. As stem-loop IV stimulates nucleotide and repeat addition processivity (Lai *et al*, 2003), we also tested whether this structure would bind mononucleotides. However, no changes in the imino region were observed when we titrated dGTP and dTTP up to 2.0 mM.

The structure of the apical loop and of the GA bulge is important for telomerase activity

Three specific structural features have been identified for stem-loop IV: (1) the apical loop forms a well-defined structure closed by a C·U base pair; (2) the GA bulge flanked by two G·C base pairs kinks the entire structure, as previously proposed (Bhattacharyya and Blackburn, 1994; Sperger and Cech, 2001); (3) the two A·U base pairs within the double helix proximal to the GA bulge are not formed making the local structure conformationally flexible. The residues contributing to the first two structural features are very highly conserved (Figure 2D). In order to assess the functional importance of these structural properties, we introduced five sets of nucleotide changes into the complete telomerase RNA and compared the activity of telomerase reconstituted with these mutants in enzymatic assays *in vitro* (Figure 4). The secondary structures of mutants Q1, D2, Q3, S4 and D5 (Figure 4) were established by selective 2′-hydroxyl acylation and primer extension (SHAPE) analysis with *N*-methylisatoic anhydride (NMIA), which reacts preferentially with the 2′-OH of structurally unconstrained nucleotides (Merino *et al*, 2005; Wilkinson *et al*, 2005) (Figure 5), and by NMR (2D water NOESY for the mutant RNAs; Supplementary Figure 4). The SHAPE analysis of wild-type stem-loop IV in full-length TER is consistent with the NMR structure: (1) in the heptaloop, the stacked C132–C134 nucleotides have relatively lower reactivity (weaker bands) to NMIA than U135–U138, which are much more dynamic in the structure; (2) the GA bulge is exposed and highly reactive, and the two G·C base pairs next to it are well-defined (almost no reactivity to NMIA for nucleotides C120 and C123, whereas the bands of G146–G147 have the same intensity as those in the DMSO control); (3) the two A·U base pairs proximal to the GA bulge have enhanced reactivity toward NMIA, indicating local conformational flexibility; (4) nucleotides U125–U127 are susceptible to modification, consistent with alternative base pairing in

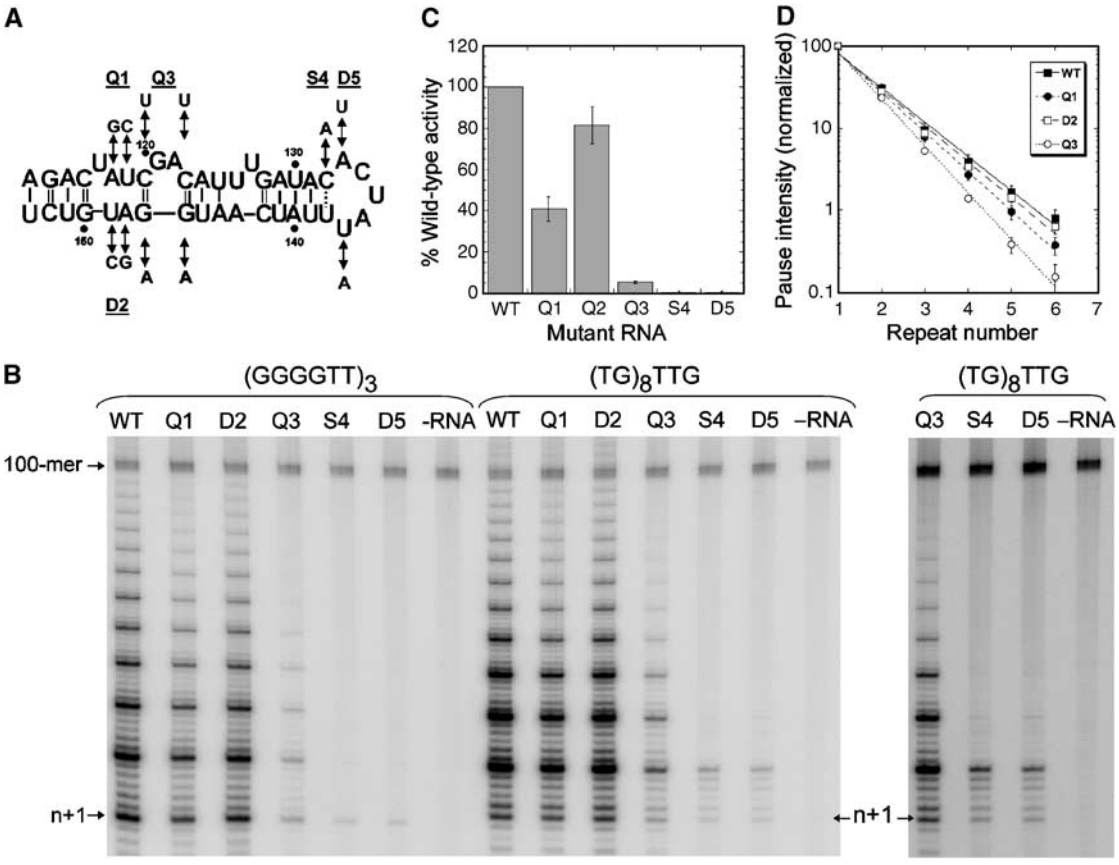

Figure 4 Enzymatic activity of mutated variants of stem-loop IV. (**A**) Locations of five sets of mutations on the stem-loop IV secondary structure. Q1, quadruple mutation: A118G/U119C/A148G/U149C; D2, double mutation: A148G/U149C; Q3, quadruple mutation: C120U/C123U/G146A/G147A; S4, single mutation: C132A; D5, double mutation: A133U/U137A. (**B**) Activity assays performed with immunopurified telomerase reverse transcriptase assembled with wild-type or mutant telomerase RNAs. Two different primers were used in the assays for comparison. 100-mer represents an end-labeled loading and recovery control; $n+1$ indicates the first nucleotide added to each primer. The panel on the right is a darker exposure of the four lanes on the right, to better illustrate the dramatic reduction in repeat addition processivity for mutants S4 and D5. (**C**) Summary of the activity of each mutant relative to wild-type telomerase RNA. The total intensity of bands in each lane was normalized to the intensity of the labeled 100-mer oligonucleotide used as a loading control. This graph is a compilation of all activity measurements with both primers and of both crude and immunopurified enzyme. Error bars represent 95% confidence intervals ($1.9 \times$ s.e.m.). (**D**) Repeat addition processivity of telomerase reconstituted with mutant RNAs. The processivity is inversely related to the slope of the line. This graph is for reactions with $(GGGGTT)_3$ primer (results obtained with the other primer were similar). Error bars represent 95% confidence intervals ($1.9 \times$ s.e.m.). The processivity of mutants S4 and D5 is negligible and therefore not presented.

the region observed by NMR, whereas the stacked bases A143–U145 are not reactive to NMIA.

Consistent with previous studies (Sperger and Cech, 2001; Lai *et al*, 2003; Mason *et al*, 2003), changing the sequence of loop residues has the most profound effect on both telomerase activity and processivity. Two sets of mutations (C132A; S4) and (A133U, U137A; D5) were introduced: S4 investigates the importance of the C·U base pair and D5 studies whether a second A·U base pair may form and contribute to catalysis. Both mutations drastically reduce telomerase activity (<1%) and are profoundly defective in repeat addition processivity, being almost incapable of the translocation required for addition of more than one repeat (Figure 4B, right panel). Mutant S4 replaced the C·U base pair with a more stable A·U pair, and base pair formation (U138 imino) was clearly observable in 2D water NOESY (Supplementary Figure 4). However, a possible A133–U137 base pair that could also form in the loop (according to mFOLD) and would significantly alter its conformation is not supported by the NMR nor SHAPE data: the relative intensities of bands corresponding to bases A133 and U137 are very similar to the wild type, indicating equal reactivity in the two structures (Figure 5B). Mutant D5 switches the identities of A133 and U137, and the SHAPE analysis shows that this mutation destabilizes U138 by making this nucleotide highly susceptible to modification.

Consistent with our suggestion that the absence of the base pairs in the middle helix and the resulting conformational flexibility have a moderate functional role, changing the two A·U base pairs to G·C (mutant Q1) reduces activity to ~40% of wild type, and a decrease of processivity (~2-fold) is also observed (Figure 4). These two A·U base pairs are highly conserved among *Tetrahymena* species, and are only replaced by more stable base pairs in *Colpidium* (Ye and Romero, 2002). NOE interactions linking the imino protons of the three continuous G·C base pairs in mutant Q1 demonstrate that these base pairs form in the mutant (Supplementary Figure 4), a result consistent with the SHAPE analysis (Figure 5). Furthermore, abolishing these two base pairs by mutating A148 to G and U149 to C (mutant D2) has a negligible effect on telomerase activity and processivity. The SHAPE reactivity results indicate that mutant D2 contains an unpaired internal loop between U117 and U119, but

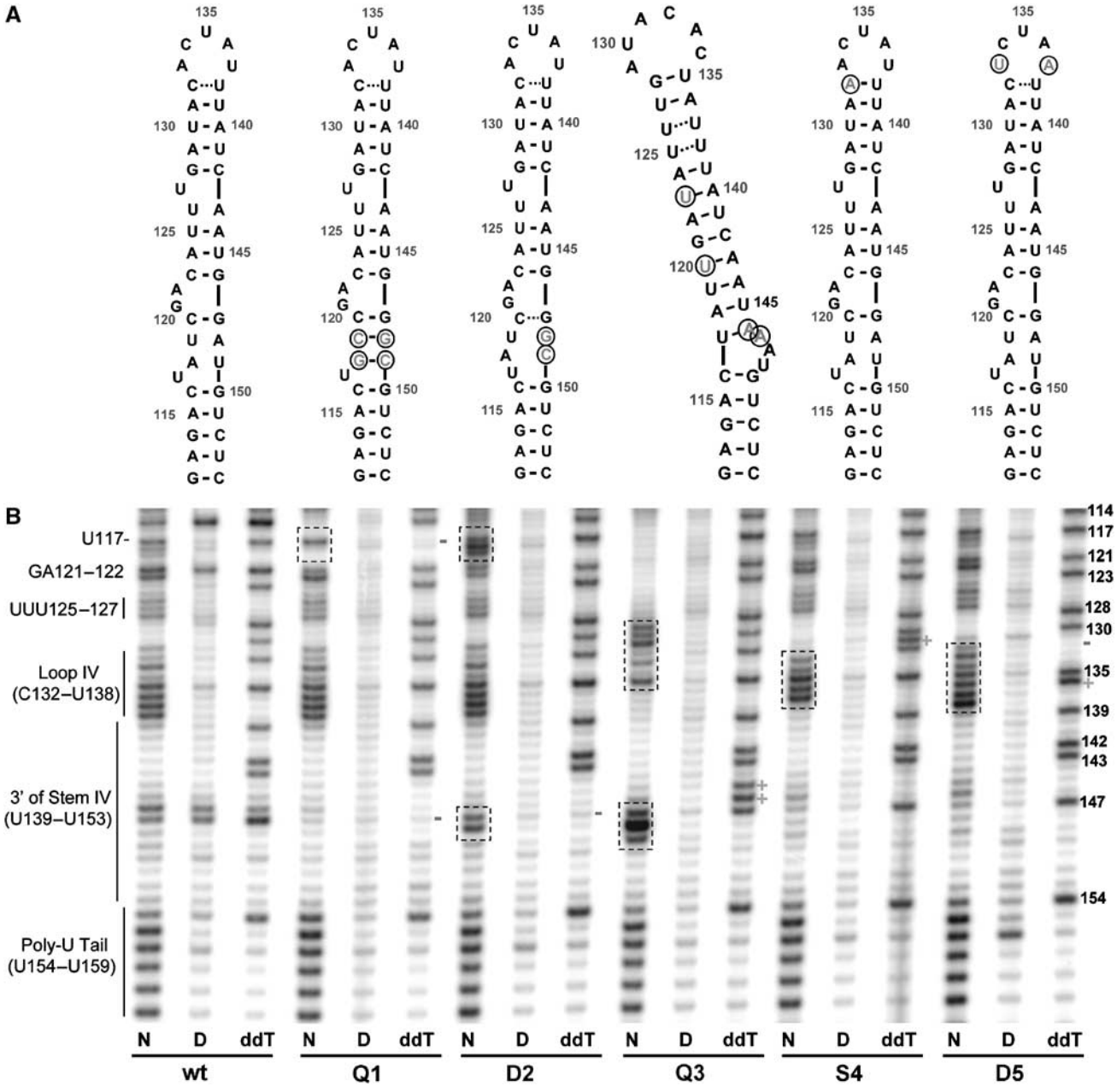

Figure 5 Secondary structures of stem-loop IV mutants. (**A**) Secondary structures of wild-type and mutant Q1, D2, Q3, S4 and D5 as determined by NMR and SHAPE analyses; the mutated nucleotides are shown in circle. (**B**) SHAPE analyses of wild-type (wt) and mutant stem-loop IV RNAs. The analysis was executed on full-length TER carrying the appropriate mutations, but only the stem-loop IV is shown for clarity. TER and the five stem-loop IV mutants were reacted with 10 mM NMIA, and the resulting 2′-acylated RNAs were mapped by reverse transcription. Sites of acylation cause reverse transcription to stop exactly one nucleotide before the modification site. The ladders are labeled to include this one-nucleotide shift for ease of interpretation. Each RNA was reacted with either NMIA (N) or the carrier DMSO (D) as labeled below each lane. Dideoxythymidine ladder (ddT) was generated to illustrate nucleotide position. The position of every added adenine (Q3: G146A, G147A; S4: C132A; D5: U137A) or removed adenine (Q1: A118G, A148G; D2: A148G; D5: A133U) for each mutant is notated by (+) or (−), respectively. Dashed boxes highlight altered nucleotide reactivity of the mutants to NMIA compared to wild type.

the G147·C120 base pair next to the GA bulge is likely to form as C120 is not susceptible to modification (Figure 5).

The GA bulge in stem-loop IV is critical for telomerase function (Sperger and Cech, 2001), and the two G·C base pairs next to the GA bulge are absolutely conserved among 17 *Tetrahymenine* species (Ye and Romero, 2002). Replacing them with A·U base pairs (mutant Q3) reduces telomerase activity 20-fold and decreases telomerase repeat addition processivity ~5-fold (Figure 4). These mutations significantly change the conformation of stem-loop IV, as demonstrated by RNA SHAPE analysis (Figure 5) and NMR (Supplementary Figure 4).

A possible explanation for the loss of activity would invoke reduced binding of TERT protein to the mutant RNAs. However, when we measured protein binding directly, none of the mutants were defective in binding to full-length TERT protein (Supplementary Figure 5A), consistent with high-affinity TERT binding being provided by a different part of

the RNA (Lai *et al*, 2001). Because a lower-affinity interaction has been reported between stem-loop IV and the N-terminal region of TERT (Lai *et al*, 2003; O'Connor *et al*, 2005), we also measured binding of the mutant stem-loop IV RNAs to a fragment of TERT encompassing amino acids 2–191 (Supplementary Figure 5B). Again, all mutants bound to this region of TERT protein as well as wild-type RNA. The interaction between this fragment of TERT and TER has been reported to be nonspecific (Jacobs *et al*, 2006), but a construct containing amino acids 1–195 possesses some specificity (O'Connor *et al*, 2005). Therefore, we cannot rule out the possibility that our mutant RNAs would be defective in binding to the slightly longer TERT fragment. Nevertheless, the protein-binding data demonstrate that these mutants are not defective in TERT recruitment.

Discussion

Stem-loop IV of *T. thermophila* telomerase RNA is a functionally critical structure: deletion of the complete stem-loop, mutations of conserved residues in the loop and deletion of the conserved G·A bulge, all dramatically affect telomerase activity (this work and Sperger and Cech, 2001; Lai *et al*, 2003; Mason *et al*, 2003). The NMR structure presented here shows that the apical part of stem IV forms a hepta-nucleotide loop with a well-defined and unique conformation that is closed by a C·U base pair. The conserved G121–A122 bulge as well as two G·C base pair next to it introduces a sharp kink in the structure, whereas two base pairs predicted to form within the template-proximal region of this RNA are not present, leading to local conformational flexibility.

The structure of the apical loop is critical for telomerase activity

We were surprised to observe a structurally well-defined loop: RNA loops of this size are generally conformationally flexible. Although six of seven nucleotides in the apical loop of stem-loop IV (the exception being C134) are conserved in all *Tetrahymenine* ciliate species examined (Ye and Romero, 2002), mutational studies (Figure 4 and previous studies (Sperger and Cech, 2001; Mason *et al*, 2003)) demonstrate that the most important loop residues for telomerase activity are those near the double helical stem. In fact, whereas U135 and U137 are the two most solvent accessible nucleotides in the loop (making them ideal candidates for direct recognition by TERT or to form tertiary interactions), the U135A mutant is only half as active as wild type (Sperger and Cech, 2001). Similarly, the Watson–Crick face of nucleotides A133 and C134 is solvent exposed, yet mutants like A133U and C134G retain nearly wild-type telomerase activity (Sperger and Cech, 2001; O'Connor *et al*, 2005). In contrast, mutations of either C132 or U138, even to other canonical or mismatched pairs (e.g. A·U (mutant S4), G·U or C·A (Sperger and Cech, 2001)) are not tolerated. Mutant S4 forms a stable A·U base pair at the base of the heptaloop, yet is defective in both telomerase activity and processivity, suggesting that a weak base pair at the base of the loop contributes to enzyme activity. Mutant D5 demonstrates that the identity of the two bases (A133 and U137) following the C·U base pair cannot be switched; SHAPE analysis demonstrate that this mutation destabilizes the C·U base pair, as U138 becomes highly reactive compared to wild type (Figure 5).

A possible role for the apical loop is in binding TERT protein, as both U137 and U138 could be crosslinked to TERT (Lai *et al*, 2003) and mutation of these two nucleotides reduced binding of the N-terminus of TERT to stem-loop IV (O'Connor *et al*, 2005). However, we did not observe any significant decrease in affinity of any of our TER mutants with full-length TERT, or with the N-terminal domain of TERT protein. This result is consistent with the observation that high-affinity binding to TERT is provided by a region near the template (Figure 1A) (Lai *et al*, 2001). Therefore, if these mutants affect telomerase activity through an interaction with TERT, as is certainly possible, they do so by affecting the conformation of the enzyme active site and not just the affinity of the protein–RNA interaction.

Bending of the structure by the GA bulge in the middle of stem IV affects catalytic activity

The GA bulge and the two G·C base pairs on either side of it are phylogenetically absolutely conserved in telomerase RNAs from 17 *Tetrahymenine* ciliates (Ye and Romero, 2002) (Figure 2D). Deletion of this bulge reduces telomerase activity nearly 20-fold, but its substitution with UU or CU restores activity (Autexier and Greider, 1998; Sperger and Cech, 2001): these results make it highly likely that the function of these nucleotides is structural. Bulged nucleotides often distort the helical axis of RNA helices (Bhattacharyya and Blackburn, 1994) and indeed we observe that the GA bulge opens up the major groove and causes a 40–45° kink in the double helix axis (Figure 2). The distortion is caused by A122 remaining stacked within the double helix while G121 is completely bulged out. The two conserved G·C base pairs next to the GA bulge are required for the correct formation of the bulge structure, as changing them to A·U pairs (mutant Q3) reduces activity 20-fold (Figure 4) and dramatically alters the central and distal stem-loop IV structure (Figure 5). This mutation is as deleterious as removing the GA bulge altogether. Deletion of the GA bulge would generate a perfectly straight and base paired helix in the middle of stem IV.

In contrast to the structurally rigid distal part of stem-loop IV, two A·U base pairs (A118–U149, U119–A148) proposed to form near the GA bulge are not observed. However, the pattern of NOE interactions suggests that base stacking still exists in this region, explaining why RNAse V1 cleaves these nucleotides poorly and DEP modifies A118 and A148 inefficiently (Bhattacharyya and Blackburn, 1994; Sperger and Cech, 2001). Mutations that abolish base-pairing for the two A·U pairs and open up the region between bulges U117 and U119 (mutant D2, U149C and A148G) have very little effect on enzyme activity and processivity, but rigidifying this region through the conservative introduction of two G·C pairs (mutant Q1) affects activity and processivity 2–3-fold. It is quite possible that these mutations would have more significant effects *in vivo* by affecting the interaction of TER with p65, a holoenzyme protein that recognizes the proximal region of stem-loop IV including the GA bulge and cooperatively improves the TERT-TER affinity (O'Connor and Collins, 2006).

Role of stem-loop IV in telomere synthesis

The catalytic cycle of telomeric repeat synthesis by telomerase involves a complex set of conformational rearrangements to position the template, substrates and product into the

enzyme active site, and to reposition the enzyme onto the template following each repeat addition. It was suggested that a dynamic structural rearrangement of the stem III pseudoknot pairing could be part of the process (Lai *et al*, 2003), and that the folding of the pseudoknot region could be influenced by interactions with stem-loop IV and with TERT (Sperger and Cech, 2001). Our results confirm that the highly structured stem IV loop closed by a unique C·U base pair is functionally very important and that the combination of rigid kinking by the GA bulge and structural flexibility in the nearby proximal stem region contribute to enzymatic activity. Activity and processivity are not significantly affected by mutations such as D2 that disrupt base pair formation completely, but are reduced by mutations that rigidify the template-proximal region of the structure. We propose that the bending at the GA bulge and the flexibility in the nearby region enables the apical loop to be repositioned during the nucleotide and repeat addition process, but they may also contribute to RNP assembly. Deletion of the GA bulge strongly (30-fold) reduces p65 enhancement of TERT RNP assembly (O'Connor and Collins, 2006; Prathapam *et al*, 2005). However, this possibility was not investigated here because the *in vitro* activity assays were conducted in crude reticulocyte lysates that lack p65.

Ciliate stem-loop IVs have been proposed to be functionally analogous to the CR4–CR5 region of vertebrate telomerases (Mason *et al*, 2003) and to a hairpin from the telomerase RNA of the budding yeast *Kluyveromyces lactis* (Roy *et al*, 1998). Are the ciliate and human telomerase RNA structures also structurally related? A stem-loop called P6.1 within human CR4–CR5 is required for TERT binding and is critical for telomerase activity *in vitro* and *in vivo* (Mitchell and Collins, 2000). Just like the apical loop of *T. thermophila* stem-loop IV, loop P6.1 has a rigid and well-defined conformation stabilized by a G·U wobble pair formed by two of the five unpaired loop residues (Leeper *et al*, 2003). It is also near a three-way junction that we have observed to be in conformational exchange by NMR (data not shown). We propose that this junction plays the same structural and functional role as the template-proximal section of stem-loop IV, by providing a flexible joint to position loop P6.1.

Materials and methods

RNA preparation

Three oligonucleotides were prepared for structural determination (Supplementary Figure 1): (1) Tet43-full, nucleotides 113–153 plus an extra G·C for synthetic reasons; (2) Tet43-top, nucleotides 123–146 plus two G·C base pairs; (3) Tet43-bot, nucleotides 113–125 and 144–153, capped by a CUUCGG tetraloop for stability, plus an extra G·C base pair. All RNAs were synthesized by *in vitro* transcription using T7 RNA polymerase and synthetic DNA templates (IDT) with commercially available unlabeled or $^{13}C/^{15}N$ labeled nucleotides (Silantes). All RNA samples were purified as described (Price *et al*, 1998). Dialysis was used to bring the final buffer to 10 mM Na-phosphate (pH 6.0) with 0.1 mM EDTA. Freeze-dried RNAs were redissolved in 5% D_2O/95% H_2O or 100% D_2O. For the tet43-full, selective labeling ($^{13}C/^{15}N$ labels only for A and C or G and U) was used to reduce spectral overlap. Samples used for RDC measurements were dialyzed into 10 mM Na-succinate (pH 6.0) and mixed with Pf1 phage (ASLA Ltd.) dialyzed against the same buffer at a final phage concentration of 12–15 mg/ml.

Data collection and analysis

Most NMR data were acquired on Bruker 500 MHz DRX or 750 MHz DMX spectrometers equipped with conventional HCN probes. Three-dimensional NOESY-HSQC experiments were collected at PNNL (Richland, WA) on a Varian 600 MHz spectrometer equipped with a cryo-probe. Data were processed with nmrPipe (Delaglio *et al*, 1995) and analyzed with Sparky (Goddard and Kneller).

Spectral assignments initiated by standard 2D NOESY were extended using 3D NOESY-HSQC experiments (Varani *et al*, 1996). Base pairs were established from the 2D water NOESY collected with Watergate water suppression and by HNN-COSY experiments (Dingley and Grzesiek, 1998; Pervushin *et al*, 1998). Dihedral angle restraints were obtained from 2D and 3D-TOCSY, $^{1}H/^{31}P$ HETCOR and 3D HCP spectra (Varani *et al*, 1996). In-Phase-Anti-Phase HSQC spectra (IPAP) (Andersson *et al*, 1998) for RDC measurement were collected at 500 MHz and 25°C on the AC- and GU-labeled full-length samples. ^{13}C $T_{1\rho}$ of the C6 of pyrimidines and C8 of purine were recorded as a series of 2D spectra at 500 MHz with constant time acquisition, and calculated as described (Shajani and Varani, 2005).

Structure determination

NOEs involving nonexchangeable protons were classified as strong (1.8–3.2 Å), medium (2.2–4.2 Å), weak (2.5–5.5 Å) or very weak (3.0–7.0 Å) based on cross-peak intensities at 100 and 200 ms mixing times (2D NOESYs) and 120 ms (3D NOESYs). NOEs involving exchangeable protons were characterized as strong (1.8–3.4 Å), medium (1.8–4.5 Å), weak (1.8–6.0 Å) and very weak (1.8–6.5 Å) based on their NOE cross-peak intensities at 100 and 200 ms mixing times. Each experimentally determined G·C base pair was constrained by six hydrogen bonding distance restraints, and each A·U base pair by four. Weak base-pair planarity restraints that allow propeller twist and standard hydrogen-bonding restraints were used for unambiguously established base pairs. The ribose conformations and the other backbone torsion angles were established and restrained by using methods as described (Varani *et al*, 1996). Constraint statistics are shown in Table I.

RDCs were calculated using the method as described (Leeper and Varani, 2005). However, separate grid searches for D_a and R were carried out for the apical part, the proximal stem and the complete molecule, to establish whether there was significant interdomain motion. The final values of the orientation parameters were very close (within 5%) for each of the three fragments: therefore, the extent of dynamic reorientation between the top and bottom part of the RNA structure is small and a single-axis system and common alignment tensor were used to refine the final RNA full-length structure.

A single extended starting structure was generated within Xplor-NIH (Schwieters *et al*, 2003) and initial velocities were randomized for each of 100 distinct structures that were subjected to torsion angle dynamics and simulated annealing. RDC-derived restraints were added only after the majority of converged structures were found to be consistent with the NOE and dihedral constraints. Only RDCs obtained from the well-ordered residues, 112–116, 123–125, 128–131, 139–142, 143–146, 150–154, were used in the refinement.

Telomerase activity

A plasmid (pTet-telo) containing the *Tetrahymena* telomerase RNA gene was a gift from Art Zaug (Zaug and Cech, 1995). Plasmids encoding mutant telomerase RNAs were constructed by site-directed mutagenesis of pTet-telo and confirmed by sequencing. Wild-type and mutant plasmids were transcribed *in vitro* and the RNAs were isolated by gel-purification as described (Bryan *et al*, 2000).

FLAG-tagged *Tetrahymena* TERT (Bryan *et al*, 2003) was translated in a rabbit reticulocyte lysate reaction using the TnT Quick for PCR kit (Promega), and 9 μl of the translation reaction were added to 1 μl wild-type or mutant telomerase RNA (final concentrations of 2 and 20 nM). The reaction was incubated at 30°C for 10 min to allow for complex formation. Telomerase activity was initiated by addition of reaction buffer (Bryan *et al*, 2000), 2.5 μM of the indicated DNA primer, 100 μM dTTP and 10 μM [α-^{32}P]dGTP at 80 Ci/mmol (Perkin-Elmer). The reaction was incubated at 30°C for 60 min and then electrophoresed on a 10% polyacrylamide/8 M urea gel. A 100-mer DNA oligonucleotide labeled with T4 polynucleotide kinase and [γ-^{32}P]ATP was added to the reaction before phenol/chloroform extraction as a recovery and loading control.

Telomerase activity assays were conducted in crude reticulocyte lysates (as above) in order to circumvent quantitation problems due

to varying immunoprecipitation efficiencies. However, as there are telomerase processivity inhibitors in rabbit reticulocyte lysates (Bryan *et al*, 2000), we also measured activity of the TER mutants using immunopurified telomerase. For these reactions, the plasmid encoding FLAG-tagged TERT was translated in the presence of 20 nM telomerase RNA in 50 μl rabbit reticulocyte lysate reactions using the TnT Quick for PCR kit (Promega) at 30°C for 60 min. The telomerase complexes were then immunopurified on anti-FLAG M2 affinity gel (Sigma-Aldrich) as described (Bryan *et al*, 2000), with the exception that the buffers contained no Nonidet P-40. The immunoprecipitation efficiency was determined by electrophoresis of 5 μl of the resulting bead slurry on an 8% SDS–PAGE gel, and an equal amount of precipitated protein was included in telomerase activity assays as described above, with the exception that these reactions contained 1 μM each of DNA primer. The relative activities of wild-type and mutant telomerases did not differ significantly between crude and purified telomerase.

Relative activity levels were quantified using ImageQuant software (GE). The total intensity of bands in each lane was normalized to the intensity of the labeled 100-mer oligonucleotide used as a loading control. Repeat addition processivity of the reactions using primer $(G_4T_2)_3$ was quantified as described (Bryan *et al*, 2000).

Binding of telomerase RNA to TERT protein

Available as Supplementary data at *The EMBO Journal* online.

RNA SHAPE analysis

RNAs for SHAPE analysis were synthesized with wild-type 5′ ends, a 3′ linker and 3′ RT primer-binding site from templates generated by PCR (Merino *et al*, 2005; Wilkinson *et al*, 2005). The 43 nucleotide 3′ extension has been shown to fold independently of TER (unreported data). RNA (1 pmol) was snap annealed in 7 μl of deionized water at 95°C for 2 min and placed on ice for 5 min before 2 μl of 5 × TER Hit Buffer (250 mM Hepes pH 8.0, 10 mM $MgCl_2$) was added. The RNA solution was then incubated at 30°C for 5 min, treated immediately with 1 μl of 100 mM *N*-methylisatoic anhydride (NMIA-Molecular Probes) in DMSO or DMSO only as a control, incubated at 30°C for 90 min, precipitated with ethanol in the presence of 0.2 M NaCl and 200 μg/ml glycogen, and reconstituted in 5 μl of TE (pH 8.0). Hit RNA (5 μl) was mapped by reverse transcription using 5′-^{32}P-labeled DNA primer (1 pmol, 5′-GAACCG GACCGAAGCCCG). The primer was annealed by heating to 95°C for 1 min, 65°C for 6 min, 35°C for 10 min, and on ice for 5 min followed by the addition of 2 μl of 5 × First-Strand Buffer (Invitrogen) reverse transcription buffer (250 mM Tris-Cl pH 8.3, 375 mM KCl, 15 mM $MgCl_2$), 0.5 μl 10 mM dNTP mix and 0.5 μl 100 mM DTT. The solution was heated to 52°C for 1 min, Superscript III reverse transcriptase (100 units; Invitrogen) was immediately added, and allowed to extend for exactly 3 min at 52°C. The reaction was quenched by the addition of 2.5 μl of 1 M NaOH, heated at 95°C for 5 min, neutralized by the addition of 2.5 μl of 1 M HCl, ethanol precipitated and resuspended in 5 μl denaturing formamide loading buffer (75% formamide, 45 mM Tris/borate, 5 mM EDTA, 0.01% bromophenol blue and xylene cyanol). Dideoxythymidine sequencing ladders were generated by incorporating 0.5 mM ddTTP in the reverse transcription reaction of unmodified TERs. The radiolabeled extension products were separated by electrophoresis on 8% denaturing sequencing gels and visualized by phosphorimaging using ImageQuant 5.1. Individual band intensities of NMIA and DMSO lanes were integrated using SAFA (Das *et al*, 2005).

Accession codes

Coordinates have been deposited in the Protein Data Bank with the following accession code 2FEY.

Supplementary data

Supplementary data are available at *The EMBO Journal* Online.

Acknowledgements

We thank EMSL-PNNL for access to NMR instruments and Dr Nancy Isern (PNNL) for help with data acquisition; Dr Thomas Leeper for assistance with the NMR spectroscopy and structural calculation; Ms Zahra Shajani for help with the $T_{1\rho}$ measurements; Julie Jurczyluk for technical assistance on the telomerase activity assay; Drs Steven Jacobs, Elaine Podell, Art Zaug and Thomas Cech for the kind gifts of the TEN protein and TER plasmid. This work was supported in part by a grant from the NSF to MBJ, the Wellcome Trust (TMB, Senior Research Fellowship GR066727MA) and the NIH-NCI and the Human Frontier of Science to GV.

Competing interests statement

The authors declare that they have no competing financial interests.

References

Al-Hashimi HM, Gosser Y, Gorin A, Hu W, Majumdar A, Patel DJ (2002) Concerted motions in HIV-1 TAR RNA may allow access to bound state conformations: RNA dynamics from NMR residual dipolar couplings. *J Mol Biol* **315:** 95–102

Allain FHT, Varani G (1995) Divalent metal ion binding to a conserved wobble pair defining the upstream site of cleavage of group I self-splicing introns. *Nucleic Acids Res* **23:** 341–350

Andersson P, Nordstrand K, Sunnerhagen M, Liepinsh E, Turovskis I, Otting G (1998) Heteronuclear correlation experiments for the determination of one-bond coupling constants. *J Biomol NMR* **11:** 445–450

Autexier C, Greider CW (1998) Mutational analysis of the *Tetrahymena* telomerase RNA: identification of residues affecting telomerase activity *in vitro*. *Nucleic Acids Res* **26:** 787–795

Bhattacharyya A, Blackburn EH (1994) Architecture of telomerase RNA. *EMBO J* **23:** 5721–5731

Blasco MA, Gasser SM, Lingner J (1999) Telomeres and telomerase. *Genes Dev* **13:** 2353–2359

Blasco MA, Lee HW, Hande MP, Samper E, Lansdorp PM, DePinho RA, Greider CW (1997) Telomere shortening and tumor formation by mouse cells Lacking telomerase RNA. *Cell* **91:** 25–34

Bryan TM, Goodrich KJ, Cech TR (2000) A mutant of *Tetrahymena* telomerase reverse transcriptase with increased processivity. *J Biol Chem* **275:** 24199–24207

Bryan TM, Goodrich KJ, Cech TR (2003) *Tetrahymena* telomerase is active as a monomer. *Mol Biol Cell* **14:** 4794–4804

Cate JH, Hanna RL, Doudna JA (1997) A magnesium ion core at the heart of a ribozyme domain. *Nat Struct Biol* **4:** 553–558

Chen JL, Blasco MA, Greider CW (2000) Secondary Structure of vertebrate telomerase RNA. *Cell* **100:** 503–514

Chen JL, Keyer Opperman K, Greider CW (2002) A critical stem-loop structure in the CR4–CR5 domain of mammalian telomerase RNA. *Nucleic Acids Res* **30:** 592–597

Cruse WBT, Saludijan P, Biala E, Strazewski P, Prangé T, Kennard O (1994) Structure of a mispaired RNA double helix at 1.6 Å resolution and implications for the prediction of RNA secondary structure. *Proc Natl Acad Sci USA* **91:** 4160–4164

Das R, Laederach A, Pearlman SM, Herschlag D, Altman RB (2005) SAFA: semi-automated footprinting analysis software for high-throughput quantification of nucleic acid footprinting experiments. *RNA* **11:** 344–354

Delaglio F, Grzesiek S, Vuister GW, Zhu G, Pfeifer J, Bax A (1995) NMRPipe: a multidimensional spectral processing system based on UNIX pipes. *J Biomol NMR* **6:** 277–293

de Lange T, Jacks T (1999) For better or worse? Telomerase inhibition and cancer. *Cell* **98:** 273–275

De Lano WL (2002) *The PyMOL Molecular Graphics System*. San Carlos USA: Delano Scientific

Dingley AJ, Grzesiek S (1998) Direct observation of hydrogen bonds in nucleic acid base pairs by internucleotide $^2J_{NN}$ couplings. *J Am Chem Soc* **120:** 8293–8297

Feng J, Funk WD, Wang SS, Weinrich SL, Avilion AA, Chiu CP, Adams RR, Chang E, Allsopp RC, Yu Y, Le S, West MD, Harley CB, Andrews WH, Greider CW, Villeponteau B (1995) The RNA component of human telomerase. *Science* **269:** 1236–1241

Goddard TD, Kneller DG (2003) *Sparky 3*. San Francisco: University of California

Greatorex J, Gallego J, Varani G, Lever A (2002) Structure and stability of wild-type and mutant RNA internal loops from the SL-1 domain of the HIV-1 packaging signal. *J Mol Biol* **322:** 543–557

Jacobs SA, Podell ER, Cech TR (2006) Crystal structure of the essential N-terminal domain of telomerase reverse transcriptase. *Nat Struct Mol Biol* **13:** 218–225

Koradi R, Billeter M, Wüthrich K (1996) MOLMOL: a program for display and analysis of macromolecular structures. *J Mol Graph* **14:** 51–55

Lai CK, Miller MC, Collins K (2003) Roles for RNA in telomerase nucleotide and repeat addition processivity. *Mol Cell* **11:** 1673–1683

Lai CK, Mitchell JR, Collins K (2001) RNA binding domain of telomerase reverse transcriptase. *Mol Cell Biol* **21:** 990–1000

Lavery R, Sklenar H (1988) The definition of generalized helicoidal parameters and of axis curvature for irregular nucleic acids. *J Biomol Struct Dyn* **6:** 63–91

Lee HW, Blasco MA, Gottlieb GJ, Horner JWI, Greider CW, DePinho RA (1998) Essential role of mouse telomerase in highly proliferative organs. *Nature* **392:** 569–574

Leeper T, Leulliot N, Varani G (2003) The solution structure of an essential stem-loop of human telomerase RNA. *Nucleic Acids Res* **31:** 2614–2621

Leeper TC, Varani G (2005) The structure of an enzyme-activating fragment of human telomerase RNA. *RNA* **11:** 394–403

Lingner J, Cech TR (1998) Telomerase and chromosome end maintenance. *Curr Opin Gen Dev* **8:** 226–232

Lingner J, Hendrick LL, Cech TR (1994) Telomerase RNAs of different ciliates have a common secondary structure and a permuted template. *Genes Dev* **8:** 1984–1998

Lingner J, Hughes TR, Shevchenko A, Mann M, Lundblad V, Cech TR (1997) Reverse transcriptase motifs in the catalytic subunit of telomerase. *Science* **276:** 561–567

Lukavsky PJ, Kim I, Otto GA, Puglisi JD (2003) Structure of HCV IRES domain II determined by NMR. *Nat Struct Biol* **10:** 1033–1038

Mason DX, Goneska E, Greider CW (2003) Stem-loop IV of *Tetrahymena* telomerase RNA stimulates processivity in *trans*. *Mol Cell Biol* **23:** 5606–5613

Merino EJ, Wilkinson KA, Coughlan JL, Weeks KM (2005) RNA structure analysis at single nucleotide resolution by selective 2'-hydroxyl acylation and primer extension (SHAPE). *J Am Chem Soc* **127:** 4223–4231

Mitchell JR, Cheng J, Collins K (1999) A Box H/ACA small nucleolar RNA-like domain at the human telomerase RNA 3' end. *Mol Cell Biol* **19:** 567–576

Mitchell JR, Collins K (2000) Human telomerase action requires two independent interactions between telomerase RNA and telomerase reverse transcriptase. *Mol Cell* **6:** 361–371

O'Connor CM, Collins K (2006) A novel RNA binding domain in *Tetrahymena* telomerase p65 initiates hierarchical assembly of *Telomerase* holoenzyme. *Mol Cell Biol* **26:** 2029–2036

O'Connor CM, Lai CK, Collins K (2005) Two purified domains of telomerase reverse transcriptase reconstitute sequence-specific interactions with RNA. *J Biol Chem* **280:** 17533–17539

Pervushin K, Ono A, Fernandez C, Szyperski T, Kainosho M, Wüthrich K (1998) NMR scalar coupling across Watson–Crick base pair hydrogen bonds in DNA observed by transverse relaxation-optimized spectroscopy. *Proc Natl Acad Sci USA* **95:** 14147–14151

Prathapam R, Witkin KL, O'Connor CM, Collins K (2005) A telomerase holoenzyme protein enhances telomerase RNA assembly with telomerase reverse transcriptase. *Nat Stru Mol Biol* **12:** 252–257

Price SR, Oubridge C, Varani G, Nagai K (1998) Preparation of RNA–protein complexes for X-ray crystallography and NMR. In *RNA–Protein Interaction: Practical Approach*, Smith C (ed.) pp 37–74. Oxford: Oxford University Press

Roy J, Fulton TB, Blackburn EH (1998) Specific telomerase RNA residues distant from the template are essential for telomerase function. *Genes Dev* **12:** 3286–3300

Schwieters CD, Kuszewski JJ, Tjandra N, Clore GM (2003) The Xplor-NIH NMR molecular structure determination package. *J Magn Res* **160:** 65–73

Seto AG, Zaug AJ, Sobel SG, Wolin SL, Cech TR (1999) *Saccharomyces cerevisiae* telomerase is an Sm small nuclear ribonucleoprotein particle. *Nature* **401:** 177–180

Shajani Z, Varani G (2005) ^{13}C NMR relaxation studies of RNA base and ribose nuclei reveal a complex pattern of motions in the RNA binding site for human U1A protein. *J Mol Biol* **349:** 699–715

Sperger JM, Cech TR (2001) A stem-loop of *Tetrahymena* telomerase RNA distant from the template potentiates RNA folding and telomerase activity. *Biochemistry* **40:** 7005–7016

Tesmer VM, Ford LP, Holt SE, Frank BC, Yi X, Aisner DL, Ouellette M, Shay JW, Wright WE (1999) Two inactive fragments of the integral RNA cooperate to assemble active telomerase with the human protein catalytic subunit (hTERT) i*n vitro*. *Mol Cell Biol* **19:** 6207–6216

Varani G, Aboul-ela F, Allain FHT (1996) NMR investigations of RNA structure. *Progr NMR Spectr* **29:** 51–127

Wang C, Meier UT (2004) Architecture and assembly of mammalian H/ACA small nucleolar and telomerase ribonucleoproteins. *EMBO J* **23:** 1857–1867

Wilkinson KA, Merino EJ, Weeks KM (2005) RNA SHAPE chemistry reveals nonhierarchical interactions dominate equilibrium structural transitions in tRNA(Asp) transcripts. *J Am Chem Soc* **127:** 4659–4667

Witkin KL, Collins K (2004) Holoenzyme proteins required for the physiological assembly and activity of telomerase. *Genes Dev* **17:** 1107–1118

Ye AJ, Romero DP (2002) Phylogenetic relationship amongst tetrahymenine ciliates inferred by a comparison of telomerase RNAs. *Inter J System Evol Microbiol* **52:** 2297–2302

Zappulla DC, Cech TR (2004) Yeast telomerase RNA: a flexible scaffold for protein subunits. *Proc Natl Acad Sci USA* **101:** 10024–10029

Zappulla DC, Goodrich K, Cech TR (2005) A miniature yeast telomerase RNA functions *in vivo* and reconstitutes activity *in vitro*. *Nat Struct Mol Biol* **12:** 1272–1277

Zaug AJ, Cech TR (1995) Analysis of the structure of *Tetrahymena* nuclear RNAs *in vivo*: Telomerase RNA, the self-splicing rRNA intron and U2 snRNA. *RNA* **1:** 363–374

